

Article

Semiconducting Polymer Nanowires with Highly Aligned Molecules for Polymer Field Effect Transistors

Keon Joo Park ^{1,†}, Chae Won Kim ^{1,†}, Min Jae Sung ¹, Jiyoul Lee ^{2,3,*}  and Young Tea Chun ^{1,*}

¹ Division of Electronics and Electrical Information Engineering, College of Engineering, Korea Maritime and Ocean University, Busan 49112, Korea; kj_park0825@g.kmou.ac.kr (K.J.P.); vooxs071@g.kmou.ac.kr (C.W.K.); should357@g.kmou.ac.kr (M.J.S.)

² Department of Smart Green Technology Engineering, Pukyong National University, Busan 48513, Korea

³ Department of Nanotechnology Engineering, Pukyong National University, Busan 48513, Korea

* Correspondence: jiyoul_lee@pknu.ac.kr (J.L.); ytc24@kmou.ac.kr (Y.T.C.)

† These authors contributed equally to this work.

Abstract: Conjugated polymers have emerged as promising materials for next-generation electronics. However, in spite of having several advantages, such as a low cost, large area processability and flexibility, polymer-based electronics have their own limitations concerning low electrical performance. To achieve high-performance polymer electronic devices, various strategies have been suggested, including aligning polymer backbones in the desired orientation. In the present paper, we report a simple patterning technique using a polydimethylsiloxane (PDMS) mold that can fabricate highly aligned nanowires of a diketopyrrolopyrrole (DPP)-based donor–acceptor-type copolymer (poly (diketopyrrolopyrrole-*alt*-thieno [3,2-*b*] thiophene), DPP-DTT) for high-performance field effect transistors. The morphology of the patterns was controlled by changing the concentration of the DPP-based copolymer solution (1, 3, 5 mg mL⁻¹). The molecular alignment properties of three different patterns were observed with a polarized optical microscope, polarized UV-vis spectroscopy and an X-ray diffractometer. DPP-DTT nanowires made with 1 mg mL⁻¹ solution are highly aligned and the polymer field-effect transistors based on nanowires exhibit more than a five times higher charge carrier mobility as compared to spin-coated film-based devices.

Keywords: conjugated polymers; patterning; nanowires; molecular alignment; polymer field-effect transistors



check for updates

Citation: Park, K.J.; Kim, C.W.; Sung, M.J.; Lee, J.; Chun, Y.T.

Semiconducting Polymer Nanowires with Highly Aligned Molecules for Polymer Field Effect Transistors.

Electronics **2022**, *11*, 648. <https://doi.org/10.3390/electronics11040648>

Academic Editor: Antonio Di Bartolomeo

Received: 26 January 2022

Accepted: 17 February 2022

Published: 18 February 2022

Publisher's Note: MDPI stays neutral with regard to jurisdictional claims in published maps and institutional affiliations.



Copyright: © 2022 by the authors. Licensee MDPI, Basel, Switzerland. This article is an open access article distributed under the terms and conditions of the Creative Commons Attribution (CC BY) license (<https://creativecommons.org/licenses/by/4.0/>).

1. Introduction

Conjugated polymer materials have attracted intense attention due to their low cost, large area processability and flexibility [1–8]. These advantages make conjugated polymers promising electronic materials for next-generation devices, such as light-emitting diodes, photodetectors, chemical sensors and solar cells [9–13]. However, polymer-based devices generally suffer from inferior electrical properties as compared to their counterparts, inorganic semiconductor-based devices. Therefore, significant efforts have been made to enhance their performance. The molecular alignment of these polymer-based devices is one of the key factors for improving electrical properties. In general, charge carriers are transported mainly along the chain backbones of polymers; thus, highly aligned polymer molecules are preferable to enhance the charge transporting properties [14–18]. Therefore, it is important to organize polymer chains into well-ordered structures. In this context, various processing strategies, including bar coating [19,20] and microchannel molding [21,22], were recently introduced for aligned one-dimensional polymer structures. However, these methods have certain limitations, such as a lack of region selectivity and poor resolution (up to micro-scale). When fabricating one-dimensional polymer nanowires, the degree of molecular alignment can be increased as the width of the wires becomes narrower due to spatial confinement. In addition, patterning polymers at the desired region can be beneficial

to reduce leakage current and crosstalk with adjacent devices [23,24]. Therefore, a new processing strategy to fabricate polymer nanowires at the desired region is necessary for high-performance polymer electronic devices. In this study, polymer nanowires (NWs) are fabricated by introducing a polydimethylsiloxane (PDMS) stamp, which has a micrometer-sized ridge/groove topography, as demonstrated in our previous work [25]. The solution splits toward the sidewalls of the groove during solvent evaporation. Hence, we can obtain two NWs in one groove. Using this method, NWs using a diketopyrrolopyrrole (DPP)-based donor-acceptor (D-A)-type conjugated copolymer (poly (diketopyrrolopyrrole-*alt*-thieno [3,2-*b*] thiophene), DPP-DTT) are successfully fabricated. The structure of polymer patterns can also be modified by changing the concentration of the polymer solution. As the concentration decreases, the residual polymer materials between the peaks of pattern decrease until the peaks are completely separated to form nanowires. Finally, polymer field-effect transistors (PFETs) based on the DPP-based conjugated copolymer NWs are fabricated into the bottom gate/bottom contact (BG/BC) structure and compared with spin-coated counterparts. The effect of solution concentration on the polymer alignment is also investigated. Patterned PFETs exhibit enhanced carrier mobility as compared to spin-coated devices. However, the performance decreases when residual materials remain, even falling below that of the spin-coated devices. These experimental results can provide a new perspective on designing polymer electronic devices.

2. Materials and Methods

2.1. Preparation of PDMS Stamps

The master mold with a ridge/groove topography was fabricated by conventional photolithography. Each ridge and groove had a width of 10 μm and a depth of 1.2 μm . The mixture of Sylgard 184 (Dow Corning, Midland, MI, USA), in a 10:1 ratio by weight the of a PDMS precursor and curing agent, was cast onto the master molds. After thermal curing at 60 $^{\circ}\text{C}$, the PDMS stamps with ridge/groove topography were separated.

2.2. Fabrication of Polymer Nanowires

For polymer solutions, DPP-DTT (Ossila, Mw = 203956, PDI = 3.09) was dissolved in 1,2-dichlorobenzene (Sigma-Aldrich, St. Louis, MO, USA), followed by stirring at 70 $^{\circ}\text{C}$ overnight. Next, 3 μL of solution was dropped on the substrates, followed by the careful lamination of PDMS stamps in ambient air. Finally, thermal annealing at 140 $^{\circ}\text{C}$ for 4 h was conducted to remove residual solvent.

2.3. Optical and Structural Characterization

The atomic force microscope (AFM) (XE-100, Park Systems, Suwon, Korea) and scanning electron microscope (SEM) (CLARA, Tescan, Brno, Czech) were used to observe the morphology of polymer nanowires, and a polarized optical microscope was used to examine the optical textures of aligned polymer nanowires. The UV-vis spectrometer (Cary 60, Agilent Technologies, Santa Clara, CA, USA) and polarizer were also used to reveal the aligned features of nanowires. The crystallinity of the spin-coated DPP-DTT film and the DPP-DTT nanowire patterns were characterized using a multi-purpose X-ray diffractometer (MP-XRD) (X'Pert PRO MPD, PANalytical, Malvern, Worcestershire, UK) with the Cu $K\alpha$ ($\lambda = 1.5405 \text{ \AA}$) emission.

2.4. Electrical Characterization

The Au/Ti source and drain electrodes were deposited with metal mask by an E-beam evaporator on the commercial SiO_2 (100 nm)/Si substrates. The heavily doped-Si was used as a bottom global gate electrode. The length of the channel was 20 μm and the width of the channel was calculated considering the period and width of the polymer patterns. Subsequently, the semiconducting polymer was spin coated or patterned on the electrode, resulting in bottom gate/bottom contact PFET configuration. The transfer and

output characteristics of the PFETs were measured by a Keithley 4200A-SCS semiconductor parameter analyzer.

3. Results and Discussion

In the first step of pattern fabrication, the PDMS stamp with a ridge/groove topography was laminated onto the droplet of polymer and slight pressure was applied during the patterning process. During the solvent evaporation process, the solution split toward the sidewalls of the grooves and formed a capillary bridge between the stamp and substrate. In addition, the contact line between the liquid bridge and the substrate was pinned by the groove. The liquid that evaporated from the edge of the capillary bridge was compensated by the liquid underneath the ridge. Hence, the solute underneath the ridge flowed towards the groove. Additionally, the pressure applied during the process continuously pushed the liquid out. Therefore, no residual polymers could be detected underneath the ridge after drying. More details of the mechanism are available in our previous research [25]. In the fabrication experiment, about 3 μL of DPP-DTT solution was drop-casted onto the substrate. After that, a 1 cm^2 sized PDMS stamp was laminated onto the droplet and dried under slight pressure at room temperature. Finally, DPP-DTT patterns were left on the substrate after removing the stamp. Since evaporation occurred from the pinning point, a small amount of solution was trapped between the precipitated solute and the sidewall during the drying process, thereby creating a gap between the wire and the sidewall of the PDMS groove after drying. This gap prevented the damage to the wire when removing the stamp. Figure 1a shows a simple comparison between the DPP-DTT-based spin-coated film and the nanowires. The alignment of the polymer backbones is discussed later in the paper. Figure 1b,c show the schematic and optical microscope image of the NW-based PFET. To investigate the effect of the concentration of the polymer solution on the surface morphology, three different polymer concentrations (1, 3, 5 mg mL^{-1}) were used to fabricate the patterns.

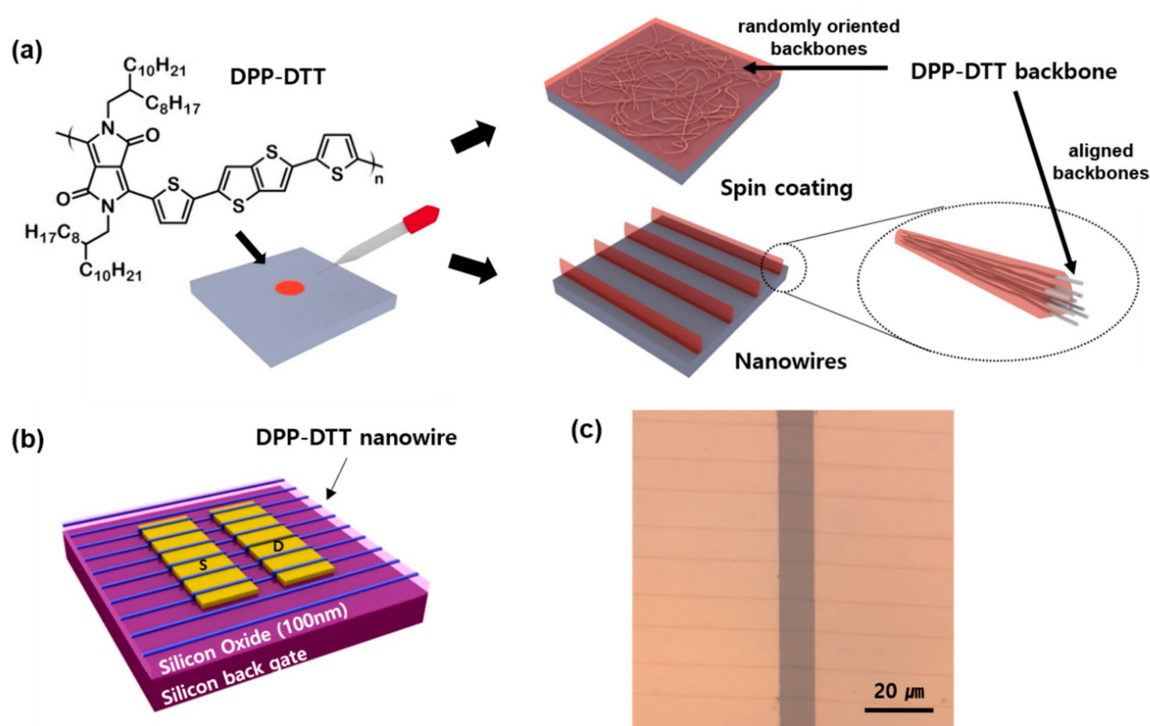


Figure 1. (a) A comparison of the DPP-DDT spin-coated film and nanowires. Spin-coated film has randomly oriented backbones and nanowires have aligned backbones. (b) Schematic and (c) optical microscope image of the DPP-DDT nanowire-based PFET.

The surface morphologies of the fabricated patterns are confirmed with AFM (Figure 2). With a solution concentration of 5 mg mL^{-1} , the patterns were almost filled inside the grooves, resulting in trapezoid-like patterns. The patterns based on the 3 mg mL^{-1} and 1 mg mL^{-1} solutions separated perfectly with no residual polymers between the wires. The widths of the patterns were $10.5 \text{ }\mu\text{m}$, $1 \text{ }\mu\text{m}$ and 670 nm for 5 mg mL^{-1} , 3 mg mL^{-1} and 1 mg mL^{-1} , respectively. The root mean square (RMS) roughness values were also extracted from the morphology measurement to confirm the existence of residual polymers. The calculated roughness values on the outside of the patterns were 0.59 , 0.57 , 0.66 nm for the solution concentrations of 1 , 3 , 5 mg mL^{-1} , respectively, which indicated that there was no residue underneath the ridge. The patterns made with 1 and 3 mg mL^{-1} exhibited equivalent roughness values (0.48 and 0.54 nm , respectively) between the wires (middle of the groove), which indicated that the solution is completely separated during process. In contrast, the roughness value between the patterns fabricated with a 5 mg mL^{-1} solution was 0.97 nm , indicating residual polymers between the patterns. These results are well matched with the mechanism of our patterning method. Moreover, no swelling or deformation of PDMS was observed under our process condition, even though PDMS is known to suffer from swelling and may have compatibility issues with some solvents, which arises from the porous nature. If swelling had occurred, there would have been residue under the ridge. Additionally, the aligned features of polymer patterns were revealed by polarized UV-vis spectroscopy. Depending on the direction of polarization, the absorption spectrum exhibited different peak intensities. These differences can be evidence of well-aligned molecules along the direction of the patterns. The degree of alignment can be quantified by the dichroic ratio (DR), which can be calculated by $\text{DR} = A_{\parallel} / A_{\perp}$, where A_{\parallel} (A_{\perp}) denotes the absorbance intensity in case the patterns are parallel (perpendicular) to the polarization [26,27]. Patterns with the width of $10.5 \text{ }\mu\text{m}$ (5 mg mL^{-1}) have a DR value of 0.81 (Figure 3a), which is less than 1. This refers to the presence of molecules that are aligned perpendicular to the direction of the patterns. The alignment of these molecules appears to be caused by the “dragging force” when the solution splits towards the sidewalls of the groove during the pattern formation. In contrast, the DR values are 1.9 and 3.7 for the $1 \text{ }\mu\text{m}$ wires (3 mg mL^{-1}) and 670 nm wires (1 mg mL^{-1}), respectively (Figure 3c,e). The higher value for the 670 nm wires suggests that the polymer molecules are better aligned. In addition, the polarized optical microscope (pOM) was also used to observe the molecular alignment of the polymer patterns [28,29]. The pOM images show a change in the brightness as the angle of the polarizer rotates (Figure 3b,d,f). The brightness was maximized when the angle between the pattern and polarizer was 45° , and minimized at 0° . This difference in brightness indicates that polymer molecules are aligned along the direction of the pattern. In the case of the 670 nm and $1 \text{ }\mu\text{m}$ wires, the patterns hardly reflected light at 0° . This extinction is the evidence of well-aligned molecules along the direction of the wire. However, the $10.5 \text{ }\mu\text{m}$ patterns were brighter than the others. This means that some molecules between the patterns were aligned perpendicular to the direction of the pattern, and this result agrees well with the DR value of the $10.5 \text{ }\mu\text{m}$ patterns. In addition, the crystallinity of the spin-coated DPP-DTT film and the DPP-based copolymer patterns were also investigated with the wide-angle, out-of-plane XRD diffraction spectrum, as shown in Figure 4. The XRD data of the spin-coated DPP-DTT film exhibited an extremely weak (100) peak. In contrast, 670 nm wide NWs obtained from DPP-DTT (1 mg mL^{-1}) showed a distinct (100) peak at $2\theta = 4.36$, corresponding to a d-spacing of 20.27 \AA . The stronger peak of the DPP-DTT 670 nm wires indicates relatively well-ordered edge-on phases in the NWs [30]. However, the (100) peak intensity decreases as the concentration increases and the $10.5 \text{ }\mu\text{m}$ patterns from the DPP-DTT (5 mg mL^{-1}) show comparable diffraction patterns with the spin-coated film because the $10.5 \text{ }\mu\text{m}$ patterns have unaligned molecules, as shown in Figure 3a,b. The higher spatial constraint of the NWs seems to be the reason for the higher degree of molecular ordering. These experimental results of pUV, pOM and XRD are well matched to each other. Overall,

these results indicate that the patterns that separated perfectly, i.e., wires, are advantageous for generating anisotropically oriented polymer molecules.

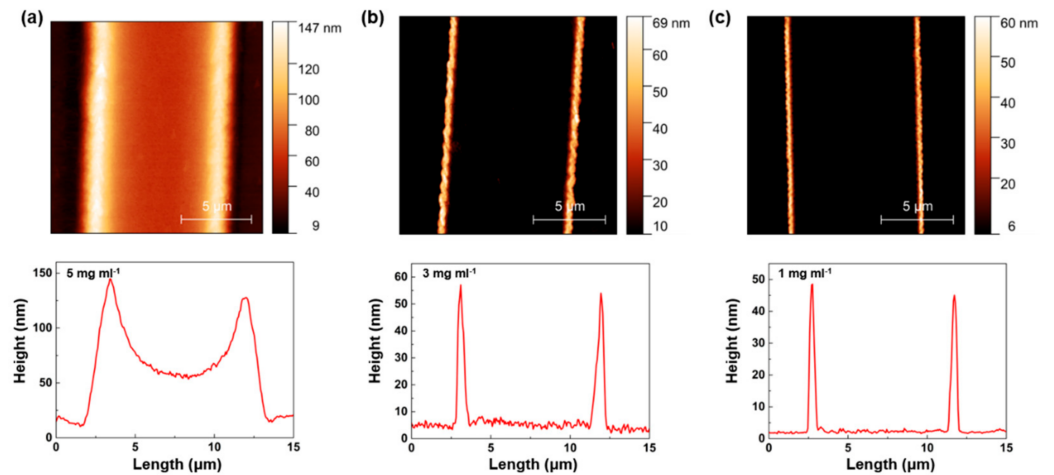


Figure 2. Atomic force microscope (AFM) image and corresponding the height profiles of the patterns fabricated with (a) 5 mg mL⁻¹, (b) 3 mg mL⁻¹ and (c) 1 mg mL⁻¹ solution. The widths of 10.5 μm, 1 μm and 670 nm were extracted from the height profiles.

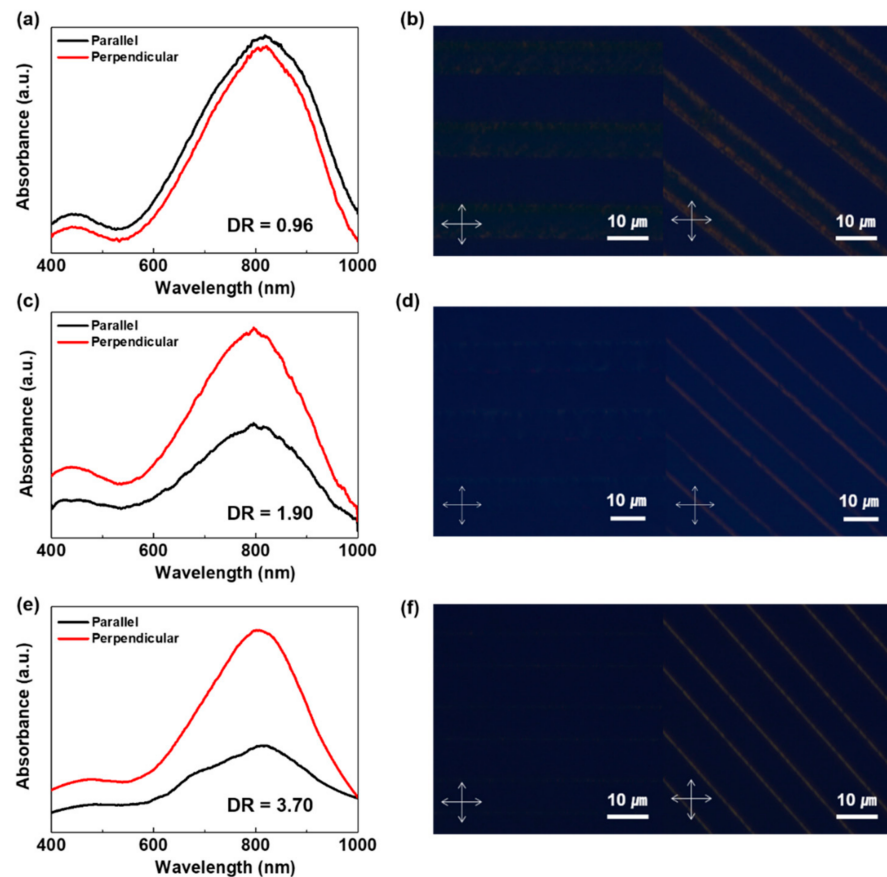


Figure 3. Polarized UV-visible absorption spectrum and polarized optical microscope image of the patterns with the widths of (a,b) 10.5 μm (5 mg mL⁻¹), (c,d) 1 μm (3 mg mL⁻¹) and (e,f) 670 nm (1 mg mL⁻¹). In the absorption spectrum, parallel (black line) and perpendicular (red line) are the angles between the patterns and the polarization directions. DR refers to the dichroic ratio. The inset arrows of the microscope images depict the direction of the crossed polarizer.

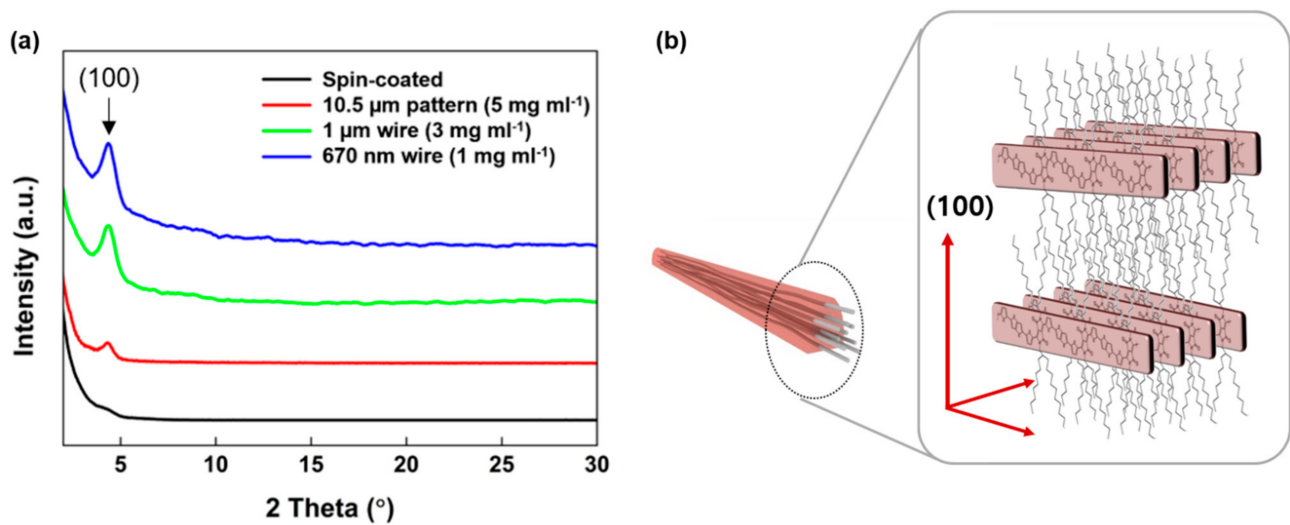


Figure 4. (a) Wide-angle XRD patterns of the spin-coated DPP-DTT film and the DPP-DTT polymer NWs on Si substrate. (b) Schematic of the edge-on phase of the DPP-DTT polymer NWs.

To evaluate the effect of molecular alignment on the electrical properties, we fabricated PFETs based on polymer patterns, including nanowires, into a BG/BC structure. For comparison, spin-coated polymer thin film was also used as an active layer for the PFETs. Figure 5 shows the typical transfer, output curves and SEM images of the devices. For all the fabricated devices, the transportation of charge carrier was effectively modulated by the gate voltage. From these electrical characteristics, we calculated the charge carrier mobilities (μ) using the following equation [31]:

$$\mu = \frac{2 \times I_{DS} \times L}{W \times C_{OX} \times (V_{GS} - V_{TH})^2} \quad (1)$$

where W and L are the channel width and length, respectively. C_{OX} is the capacitance per unit area of the gate dielectric. I_{DS} , V_{GS} and V_{TH} are the drain current, gate voltage and threshold voltage, respectively. Note that the effective channel widths of the patterned devices are calculated considering the width and period of the polymer patterns. The devices made with wires are found to exhibit enhanced mobilities as compared to spin-coated devices. However, the 10.5 μm pattern-based device shows lower mobility than the spin-coated one. This decrease in mobility is caused by the perpendicularly oriented molecules, which are mentioned above (Figure 3). During the patterning process, the gravitational force from the wall of the grooves of mold was applied to split the solution, and the direction of the force was perpendicular to the wire. The 10.5 μm patterns had more perpendicularly aligned molecules in the middle of the polymer patterns than the spin-coated film, because the polymer solution was dried under gravitational force. Since the charge carrier is transported along the wires, the perpendicularly aligned molecules disturb the transport of the charge carrier, causing a decrease in mobility. In contrast, the 3 and 1 mg mL^{-1} solutions completely separated, and no residual polymer remained between the neighbor wires. Therefore, the mobility of 1 μm (3 mg mL^{-1}) and 670 nm (1 mg mL^{-1}) wire-based devices can be improved more than the spin-coated device and 10.5 μm pattern-based device. This tendency clearly reveals that the molecular alignment is an important factor in polymer electronics. In addition, the patterned devices showed superior characteristics in terms of the gate leakage current. The spin-coated device exhibits a higher gate leakage current compared to the patterned devices, as shown in Figure 6a. Gate leakage current occurs due to the defects in the interface between the channel and dielectric film. The defects provide a conductive connection between the channel and gate electrode [32]. In the case of spin coating, the thin film covered the entire substrate; thus, the

contact interface between the dielectric layer and the channel was significantly increased. In contrast, our method enabled patterning at a desired location with a small pattern width, thereby reducing the contact area as compared to spin coating. Due to the small contact area, the gate leakage current of the 10.5 μm pattern-based device was lower than that of the spin-coated device, despite its lower mobility. This indicates that the patterning of polymers at the desired region is favorable for reducing the leakage current, regardless of its electrical performance. The threshold voltage, mobility, on/off ratio and gate leakage current are summarized in Table 1. Our DPP-DTT-based devices show low mobilities compared to recent studies, which is the result of our experimental environments. Our experiment was conducted in ambient air and we did not use any additional strategies, such as SAM treatment and a top-gate structure, which are well known to be helpful for improving the performance of PFETs, because we tried to figure out only the effect of nanowire patterning on the electrical characteristics. Note that we could observe the improvement of the electrical performance of the wire-based devices compared to the spin-coated devices, as shown in Table 1. In addition, a positive shift in the threshold voltage was observed for the patterned devices. This positive shift in the threshold voltage was affected by the oxygen infiltration to the polymer. Due to our experimental environment (ambient air), the oxygen infiltration to the polymer could easily occur. The infiltrated oxygen created the DPP-DTT- O_2 complex, which can act as an electron trap [33]. When positive bias is applied, the electrons are trapped at the DPP-DTT- O_2 complex. These trapped electrons induce p-doping, which can cause the positive shift of the threshold voltage [34]. In contrast, the V_{TH} is observed to return towards zero voltage (negative direction), as the width of the pattern decreases, as shown in Figure 6b. This phenomenon occurred because the infiltrations of oxygen were reduced due to the decreased interface area between the air and polymer materials. Less oxygen indicates a lower p-doping level, so the smaller positive shift of V_{TH} is observed for patterned devices compared to spin-coated device.

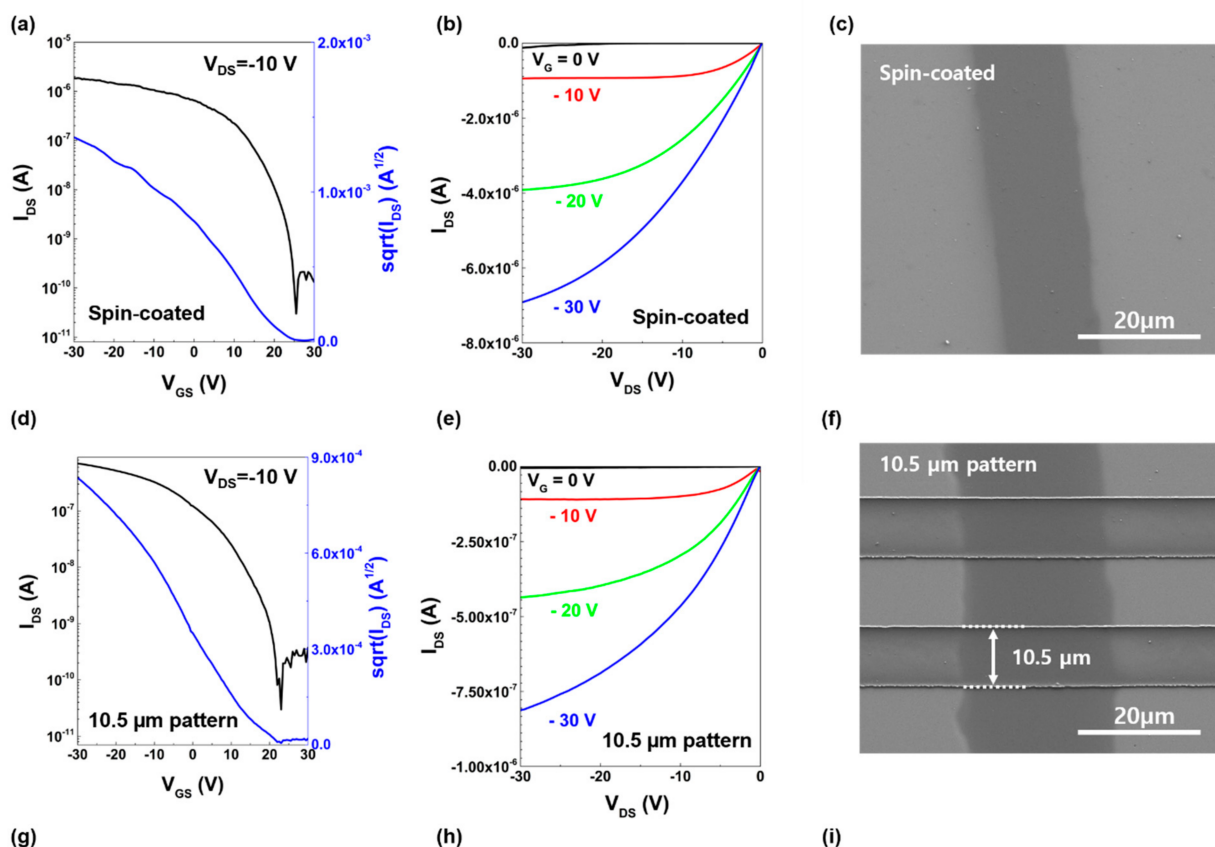


Figure 5. Cont.

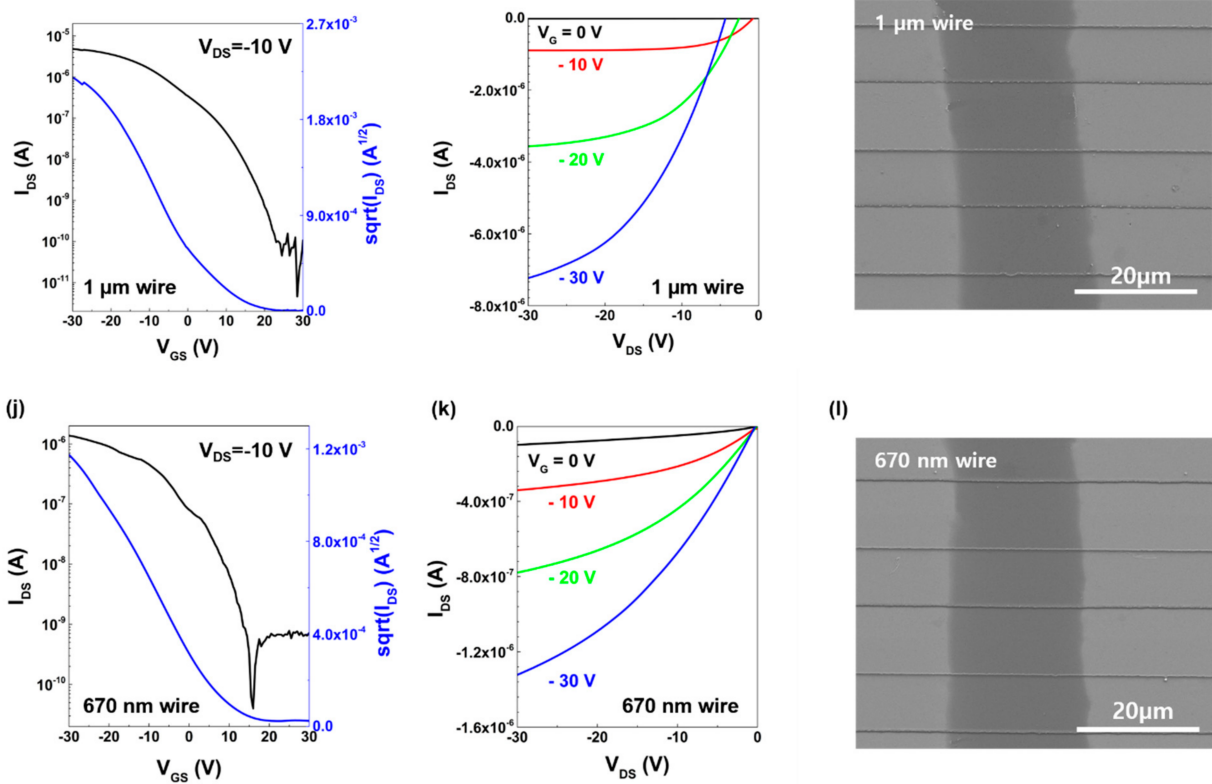


Figure 5. Typical transfer characteristics, output curves and scanning electron microscope image of (a–c) the spin-coated film-based device, (d–f) 10.5 μm patterns-based device, (g–i) 1 μm wire-based device and (j–l) 670 nm wire-based device.

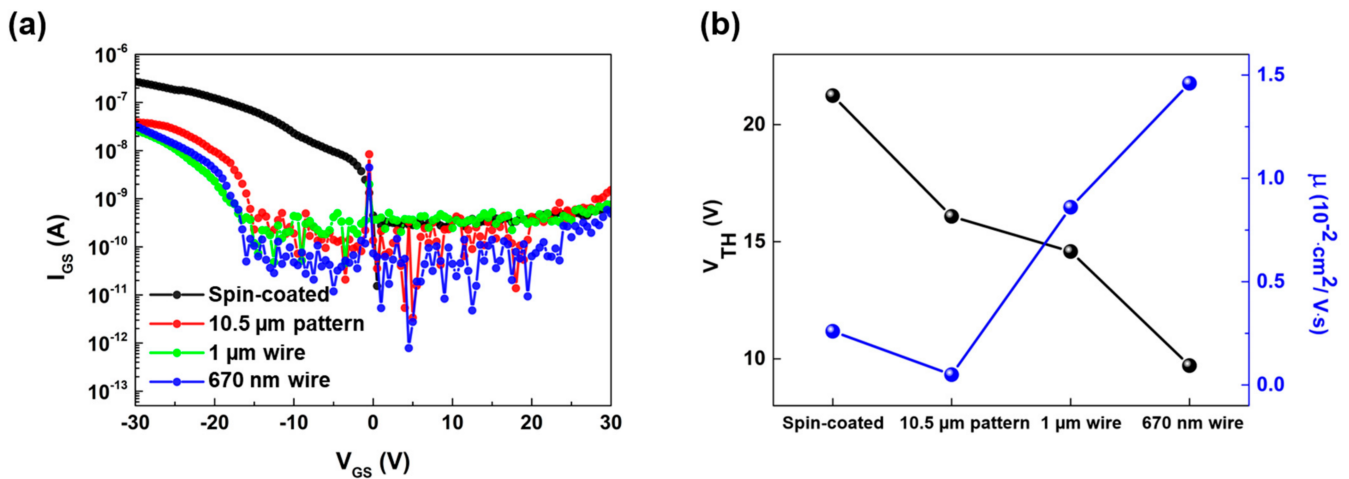


Figure 6. (a) Plot of I_{GS} (gate leakage current) versus V_{GS} ; the spin-coated device exhibits a higher gate leakage current in the range below 0 V. (b) Threshold voltage (right axis) and mobility (left axis) of the fabricated polymer field effect transistors.

Table 1. Comparison of the electrical characteristics of polymer field effect transistors.

	Threshold Voltage, V_{TH} (V)	Mobility, μ ($\text{cm}^2 \text{V}^{-1} \text{s}^{-1}$)	On/Off Current Ratio	Gate Leakage Current, I_{GS} (A)
Spin-coated	21.24	0.26×10^{-2}	$\sim 10^4$	$10^{-9} \sim 10^{-6}$
10.5 μm patterns (5 mg mL^{-1})	16.08	0.05×10^{-2}	$\sim 10^4$	$10^{-10} \sim 10^{-7}$
1 μm wires (3 mg mL^{-1})	14.58	0.86×10^{-2}	$\sim 10^5$	$10^{-10} \sim 10^{-7}$
670 nm wires (1 mg mL^{-1})	9.71	1.46×10^{-2}	$\sim 10^5$	$10^{-11} \sim 10^{-7}$

4. Conclusions

In this paper, we investigated the effect of polymer patterns on electrical properties. The polymer patterns are easily fabricated using a PDMS mold, and the morphologies of fabricated patterns were different depending on the concentration of the polymer solution. As the concentration of the polymer solution decreased, the patterns were perfectly separated and polymer nanowires with a width of 670 nm were obtained with a 1 mg mL^{-1} solution. Highly aligned molecules of DPP-DTT nanowires are confirmed by pOM and pUV-vis spectroscopy. However, 10.5 μm patterns (fabricated with a 5 mg mL^{-1} solution) exhibited an inferior molecular alignment due to the residual polymers between the patterns. The highly aligned DPP-DTT nanowires show remarkably improved electrical characteristics. The NW-based PFETs have charge carrier mobility of almost 560%, compared to the spin-coated devices. Moreover, the patterned devices also exhibit a reduced gate leakage current. In addition, the threshold voltages exhibit a positive shift for the PFETs and then decrease towards a zero point as the pattern width decreases. The oxygen infiltration is responsible for the change in V_{TH} . Our patterning method for highly aligned polymer nanowires represents a promising breakthrough to achieve high-performance electronics based on conjugated polymers.

Author Contributions: K.J.P. and C.W.K. contributed equally. Conceptualization, K.J.P., C.W.K. and Y.T.C.; analysis, K.J.P., C.W.K. and Y.T.C.; investigation, K.J.P., C.W.K. and Y.T.C.; resources, J.L. and Y.T.C.; writing—original draft preparation, K.J.P., C.W.K. and Y.T.C.; writing—review and editing, K.J.P., C.W.K., J.L. and Y.T.C.; visualization, M.J.S.; supervision, J.L. and Y.T.C.; funding acquisition, Y.T.C. All authors have read and agreed to the published version of the manuscript.

Funding: This work was supported by the National Research Foundation of Korea (NRF) grant funded by the Korea Government (MSIT) (nos. 2020R1G1A1103202, 2021R1F1A1063360 and 2021R1A2C1007212). This paper was partially supported by the Korea Institute for Advancement of Technology (KIAT) grant funded by the Korea Government (MOTIE) (P0012451, The Competency Development Program for Industry Specialist) and the Nano-Material Technology Development Program through the National Research Foundation of Korea (NRF) funded by the Ministry of Science, ICT and Future Planning (2009-0082580).

Data Availability Statement: The data that support the findings of this study are available from the corresponding authors upon reasonable request.

Conflicts of Interest: The authors declare no conflict of interest.

References

1. Drury, C.J.; Mutsaers, C.M.J.; Hart, C.M.; Matters, M.; De Leeuw, D.M. Low-Cost All-Polymer Integrated Circuits. *Appl. Phys. Lett.* **1998**, *73*, 108–110. [[CrossRef](#)]
2. Janoschka, T.; Martin, N.; Martin, U.; Friebe, C.; Morgenstern, S.; Hiller, H.; Hager, M.D.; Schubert, U.S. An Aqueous, Polymer-Based Redox-Flow Battery Using Non-Corrosive, Safe, and Low-Cost Materials. *Nature* **2015**, *527*, 78–81. [[CrossRef](#)]
3. Zhang, R.; Moon, K.S.; Lin, W.; Agar, J.C.; Wong, C.P. A Simple, Low-Cost Approach to Prepare Flexible Highly Conductive Polymer Composites by in Situ Reduction of Silver Carboxylate for Flexible Electronic Applications. *Compos. Sci. Technol.* **2011**, *71*, 528–534. [[CrossRef](#)]

4. Gao, H.; Li, J.; Zhang, F.; Liu, Y.; Leng, J. The Research Status and Challenges of Shape Memory Polymer-Based Flexible Electronics. *Mater. Horiz.* **2019**, *6*, 931–944. [[CrossRef](#)]
5. Zardetto, V.; Brown, T.M.; Reale, A.; Di Carlo, A. Substrates for Flexible Electronics: A Practical Investigation on the Electrical, Film Flexibility, Optical, Temperature, and Solvent Resistance Properties. *J. Polym. Sci. Part B Polym. Phys.* **2011**, *49*, 638–648. [[CrossRef](#)]
6. Søndergaard, R.R.; Hösel, M.; Espinosa, N.; Jørgensen, M.; Krebs, F.C. Practical Evaluation of Organic Polymer Thermoelectrics by Large-Area R2R Processing on Flexible Substrates. *Energy Sci. Eng.* **2013**, *1*, 81–88. [[CrossRef](#)]
7. Sun, C.; Pan, F.; Bin, H.; Zhang, J.; Xue, L.; Qiu, B.; Wei, Z.; Zhang, Z.G.; Li, Y. A Low Cost and High Performance Polymer Donor Material for Polymer Solar Cells. *Nat. Commun.* **2018**, *9*, 1–10. [[CrossRef](#)]
8. Tan, L.; Wang, Y.; Zhang, J.; Xiao, S.; Zhou, H.; Li, Y.; Chen, Y.; Li, Y. Highly Efficient Flexible Polymer Solar Cells with Robust Mechanical Stability. *Adv. Sci.* **2019**, *6*, 1801180. [[CrossRef](#)]
9. Zheng, H.; Zheng, Y.; Liu, N.; Ai, N.; Wang, Q.; Wu, S.; Zhou, J.; Hu, D.; Yu, S.; Han, S.; et al. All-Solution Processed Polymer Light-Emitting Diode Displays. *Nat. Commun.* **2013**, *4*, 1971. [[CrossRef](#)]
10. Gong, X.; Tong, M.; Xia, Y.; Cai, W.; Moon, J.S.; Cao, Y.; Yu, G.; Shieh, C.L.; Nilsson, B.; Heeger, A.J. High-Detectivity Polymer Photodetectors with Spectral Response from 300 Nm to 1450 Nm. *Science* **2009**, *325*, 1665–1667. [[CrossRef](#)]
11. Boussaad, S.; Tao, N.J. Polymer Wire Chemical Sensor Using a Microfabricated Tuning Fork. *Nano Lett.* **2003**, *3*, 1173–1176. [[CrossRef](#)]
12. Helgesen, M.; Søndergaard, R.; Krebs, F.C. Advanced Materials and Processes for Polymer Solar Cell Devices. *J. Mater. Chem.* **2010**, *20*, 36–60. [[CrossRef](#)]
13. Wang, G.; Melkonyan, F.S.; Facchetti, A.; Marks, T.J. All-Polymer Solar Cells: Recent Progress, Challenges, and Prospects. *Angew. Chem. -Int. Ed.* **2019**, *58*, 4129–4142. [[CrossRef](#)] [[PubMed](#)]
14. Liu, D.; Broer, D.J. Liquid Crystal Polymer Networks: Preparation, Properties, and Applications of Films with Patterned Molecular Alignment. *Langmuir* **2014**, *30*, 13499–13509. [[CrossRef](#)] [[PubMed](#)]
15. Chang, M.; Choi, D.; Egap, E. Macroscopic Alignment of One-Dimensional Conjugated Polymer Nanocrystallites for High-Mobility Organic Field-Effect Transistors. *ACS Appl. Mater. Interfaces* **2016**, *8*, 13484–13491. [[CrossRef](#)] [[PubMed](#)]
16. Wang, J.; Sun, X.; Chen, L.; Zhuang, L.; Chou, S.Y. Molecular Alignment in Submicron Patterned Polymer Matrix Using Nanoimprint Lithography. *Appl. Phys. Lett.* **2000**, *77*, 166–168. [[CrossRef](#)]
17. Chang, M.; Su, Z.; Egap, E. Alignment and Charge Transport of One-Dimensional Conjugated Polymer Nanowires in Insulating Polymer Blends. *Macromolecules* **2016**, *49*, 9449–9456. [[CrossRef](#)]
18. Luzio, A.; Martin, J.; Cheng, C.H.; Stingelin, N.; Toney, M.F.; Salleo, A.; Caironi, M. Improving Molecular Alignment and Charge Percolation in Semiconducting Polymer Films with Highly Localized Electronic States through Tailored Thermal Annealing. *J. Mater. Chem. C* **2021**, *9*, 15848–15857. [[CrossRef](#)]
19. Khim, D.; Han, H.; Baeg, K.J.; Kim, J.; Kwak, S.W.; Kim, D.Y.; Noh, Y.Y. Simple Bar-Coating Process for Large-Area, High-Performance Organic Field-Effect Transistors and Ambipolar Complementary Integrated Circuits. *Adv. Mater.* **2013**, *25*, 4302–4308. [[CrossRef](#)]
20. Lee, S.B.; Kang, B.; Kim, D.; Park, C.; Kim, S.; Lee, M.; Lee, W.B.; Cho, K. Motion-Programmed Bar-Coating Method with Controlled Gap for High-Speed Scalable Preparation of Highly Crystalline Organic Semiconductor Thin Films. *ACS Appl. Mater. Interfaces* **2019**, *11*, 47153–47161. [[CrossRef](#)]
21. Yoon, D.K.; Kim, H.; Kim, B.S.; Han, M.J.; Kim, J.; Kim, B.; Park, S.M.; Ahn, H.; Shin, T.J. Orientation Control of Semiconducting Polymers Using Microchannel Molds. *ACS Nano* **2020**, *14*, 12951–12961. [[CrossRef](#)]
22. Martin, C.R.; Aksay, I.A. Microchannel Molding: A Soft Lithography-Inspired Approach to Micrometer-Scale Patterning. *J. Mater. Res.* **2005**, *20*, 1995–2003. [[CrossRef](#)]
23. Knobloch, A.; Bernds, A.; Clemens, W. Printed Polymer Transistors. In Proceedings of the First International IEEE Conference on Polymers and Adhesives in Microelectronics and Photonics, Incorporating POLY, PEP & Adhesives in Electronics. Proceedings (Cat. No.01TH8592), Potsdam, Germany, 21–24 October 2001; pp. 84–90.
24. Balocco, C.; Majewski, L.A.; Song, A.M. Non-Destructive Patterning of Conducting-Polymer Devices Using Subtractive Photolithography. *Org. Electron.* **2006**, *7*, 500–507. [[CrossRef](#)]
25. Li, S.; Chun, Y.T.; Zhao, S.; Ahn, H.; Ahn, D.; Sohn, J.I.; Xu, Y.; Shrestha, P.; Pivnenko, M.; Chu, D. High-Resolution Patterning of Solution-Processable Materials via Externally Engineered Pinning of Capillary Bridges. *Nat. Commun.* **2018**, *9*, 393. [[CrossRef](#)] [[PubMed](#)]
26. Li, Q.Y.; Yao, Z.F.; Lu, Y.; Zhang, S.; Ahmad, Z.; Wang, J.Y.; Gu, X.; Pei, J. Achieving High Alignment of Conjugated Polymers by Controlled Dip-Coating. *Adv. Electron. Mater.* **2020**, *6*, 2000080. [[CrossRef](#)]
27. Syafutra, H.; Pandey, M.; Kumari, N.; Pandey, S.S.; Bente, H.; Nakamura, M. Assisted Alignment of Conjugated Polymers in Floating Film Transfer Method Using Polymer Blend. *Thin Solid Films* **2021**, *734*, 138814. [[CrossRef](#)]
28. Khim, D.; Luzio, A.; Bonacchini, G.E.; Pace, G.; Lee, M.-J.; Noh, Y.-Y.; Caironi, M. Uniaxial Alignment of Conjugated Polymer Films for High-Performance Organic Field-Effect Transistors. *Adv. Mater.* **2018**, *30*, 1705463. [[CrossRef](#)]
29. Lin, F.J.; Guo, C.; Chuang, W.T.; Wang, C.L.; Wang, Q.; Liu, H.; Hsu, C.S.; Jiang, L. Directional Solution Coating by the Chinese Brush: A Facile Approach to Improving Molecular Alignment for High-Performance Polymer TFTs. *Adv. Mater.* **2017**, *29*, 1606987. [[CrossRef](#)]

30. Lei, Y.; Wu, B.; Chan, W.-K.E.; Zhu, F.; Ong, B.S. Engineering Gate Dielectric Surface Properties for Enhanced Polymer Field-Effect Transistor Performance. *J. Mater. Chem. C* **2015**, *3*, 12267–12272. [[CrossRef](#)]
31. Garnier, F.; Horowitz, G.; Peng, X.; Fichou, D. An All-organic “Soft” Thin Film Transistor with Very High Carrier Mobility. *Adv. Mater.* **1990**, *2*, 592–594. [[CrossRef](#)]
32. Hengen, S.; Alt, M.; Hernandez-Sosa, G.; Giehl, J.; Lemmer, U.; Mechau, N. Modelling and Simulation of Gate Leakage Currents of Solution-Processed OTFT. *Org. Electron.* **2014**, *15*, 829–834. [[CrossRef](#)]
33. Kehrer, L.A.; Winter, S.; Fischer, R.; Melzer, C.; Von Seggern, H. Temporal and Thermal Properties of Optically Induced Instabilities in P3HT Field-Effect Transistors. *Synth. Met.* **2012**, *161*, 2558–2561. [[CrossRef](#)]
34. Zessin, J.; Xu, Z.; Shin, N.; Hamsch, M.; Mannsfeld, S.C.B. Threshold Voltage Control in Organic Field-Effect Transistors by Surface Doping with a Fluorinated Alkylsilane. *ACS Appl. Mater. Interfaces* **2019**, *11*, 2177–2188. [[CrossRef](#)] [[PubMed](#)]